In Situ Quantification of the Suspended Load of Estuarine Aggregates from Multifrequency Acoustic Inversions

G. FROMANT,[a] F. FLOC'H,[a] A. LEBOURGES-DHAUSSY,[b] F. JOURDIN,[c] Y. PERROT,[b] N. LE DANTEC,[a,d] AND C. DELACOURT[a]

[a] *Institut Universitaire Européen de la Mer, Laboratoire Géosciences Océan - UMR 6538, Plouzané, France*
[b] *Institut de la Rechercher pour le Développement, Laboratoire de l'Environnement MARin - UMR 6539, Plouzané, France*
[c] *Service Hydrographique et Océanographique de la Marine, Brest, France*
[d] *Centre d'Etudes et d'expertise sur les Risques, l'Environnement, la Mobilité et l'Aménagement, DTechEMF, Laboratoire Géosciences Océan (IUEM) - UMR 6538 CNRS-UBO, Plouzané, France*

(Manuscript received 6 April 2016, in final form 15 May 2017)

ABSTRACT

The study of the suspended particulate matter (SPM) transport is essential to understanding oceans and rivers, for their presence can impact the environment, from marine habitats or water quality degradations to important changes of the seabed morphology. Among a large number of surrogate techniques in traditional water sampling, acoustical methods have the advantage of providing nonintrusive measurements, with high spatial and temporal resolutions. However, the ability of fine-grained sediments to aggregate under the process of flocculation complexifies the interpretation of acoustical measurements. The objective of this paper is to design a simple backscattering model for flocculated sediment suspensions, in order to interpret the information provided by a multifrequency profiler and to retrieve both the concentration and the dominant size of a suspension of flocculated sediments in an estuarine context. In situ granulometry laser data, collected in the Aulne macrotidal estuary (France), showed that over the size distribution observed, a mean porosity of apparent particles in suspension can be used directly as input for model generation. The in situ acoustic signal was concurrently recorded at 0.5, 1, 2, and 4 MHz, and then inverted using the nonnegative least squares algorithm after constraining the model with an optimal porosity, allowing for a discrete representation of the mass concentration distributed over several equivalent spherical radii. The inversion results are in good agreement with the in situ mass concentration obtained through in situ water samplings.

1. Introduction

Suspended particulate matter (SPM) is ubiquitous in oceans and rivers. The study of their transport is essential, for their presence can impact the environment, from marine habitats or water quality degradations to important changes in the seabed morphology (Bilotta and Brazier 2008; Davies and Thorne 2008; Amoudry and Souza 2011).

SPM in the water column is traditionally estimated through the analysis of water samples. However, such techniques require time-consuming operations and yield measurements with limited continuity and resolution. The need to monitor and model their transport has lead scientists to design more efficient methods of SPM content estimations based on the physical properties of the suspended matter in the water column (Gray and Gartner 2009). Among a large number of surrogate techniques in traditional water sampling, acoustical methods have the advantage of providing nonintrusive measurements, with high spatial and temporal instrumental resolutions. More precisely, methods based on multifrequency acoustic backscatter measurements yield the most promising results. Through the measurement of the volume backscattering coefficients (Maclennan et al. 2002) and given a specific backscattering model that describes the scattering properties of a particle (mineral or organic), and if necessary given a specific total scattering model in case of high sediment attenuation, inversion methods have been designed and successfully applied to retrieve both the concentration and size distribution of a suspension (i.e., the heterogeneous mixture containing these particles, themselves seen as heterogeneities inside a fluid). Whether to estimate zooplankton biomass and trophic activity (Holliday et al. 1989; Holliday and Pieper 1995;

Corresponding author: Guillaume Fromant, g-fromant@hotmail.fr

DOI: 10.1175/JTECH-D-16-0079.1

Lebourges-Dhaussy et al. 2014) or non-cohesive sediment size distribution and concentration (Crawford and Hay 1993; Thorne and Hanes 2002; Thorne et al. 2011), the use of multifrequency systems has improved our knowledge of the water content of both oceans and rivers. Yet, in spite of their successful applications, the importance of an accurate backscattering model adapted to the suspension of interest still remains critical. And it requires special considerations to invert backscattered signals from suspended material of unknown scattering properties when placed in a pressure field and to retrieve a correct concentration estimate. Particularly, the ability of fine-grained sediments, usually silts or clays, to aggregate (Eisma and Li 1993; Uncles et al. 2006; Fettweis 2008; Verney et al. 2011; Manning et al. 2011) complexifies the interpretation of acoustical measurements. This process is most certainly attributed to changes of the physicochemical and/or biological properties of the surrounding medium, coupled with the phenomena of attraction/repulsion of small-sized particles placed in an agitated environment (Kranenburg 1994). These particles do possess variable sizes, shapes, and densities. Thanks to numerous observations, empirical relations between the flocs' effective densities and their size were established (Fettweis 2008; Manning et al. 2011). However, these particles are fragile and sensitive to shearing, which makes them delicate to sample and manipulate in situ without breaking them. This process is particularly intense in estuaries given the abundance of physicochemical and hydrodynamical gradients contributing to the aggregation process.

Only recently has a theoretical framework (MacDonald et al. 2013; Thorne et al. 2014) describing the interaction between sound and flocculated particles placed in controlled environment been established. It has yet to be validated in situ. The experimental observations clearly suggest that a reasonable fit between the measurements of the acoustic backscatter of a suspension of flocculated kaolin particles and the expression provided by Moate and Thorne (2009) can be achieved. Thorne et al. (2014) then suggested a backscattering model based on the transition between the solid and fluidlike behavior of the flocs as their size increase. This model provides a rational way of accounting for the behavior of the backscattered sound from a suspension of flocculated cohesive sediments. It necessitates a priori knowledge of some inherent properties of the suspension, such as the size and effective density of the flocs. Thorne et al. (2014) had access to these parameters through controlled experiments. Nevertheless, it is difficult to reproduce such measurements with natural flocs, in particular due to the difficulties encountered in situ with such fragile and easily broken aggregated particles. Applying this model to in situ suspensions thus implies a certain number of assumptions to fully constrain the inversion. These assumptions can lead to potentially erroneous interpretations of the results.

The present paper thus focuses on the implementation of a simplified inverse model based on the apparent properties of the suspension, highlighted through independent optical observations, in order to assess the possibility to invert in situ acoustic measurements. The methodology adopted here for the flocculated particles scattering model starts from the heuristic approach used to estimate the scattering characteristics of non-cohesive sandy sediment (Sheng and Hay 1988) and flocculated kaolin particles (Thorne et al. 2014). The model formulation is established with the knowledge that the suspension can be seen as the mixture of solid "apparent particles" of constant porosity with size, thus reducing the problem to one static degree of freedom, the physical properties of which (bulk density, compressional sound speed) being close to those of the sediment bed at the porous water–sediment interface, which can be estimated (Hamilton 1963; Wood 1964; Buckingham 2005). The approach presented here thus considers apparent particles, of lower density, that will account for the aggregates.

The field experiment is first presented (section 2) with the detailed survey protocol. In section 3, the optical observations are exposed, revealing the steadiness of the mean effective density of the observed aggregates over a given experiment, averaged over the total size distribution. These observations led us to formulate a new scattering model, which is described in section 4, and further used to invert the acoustic backscattering system (ABS) data. The agreement between the inverted ABS data and the in situ measurement is then exposed in section 5, and the advantages/drawbacks of the whole method are discussed in section 6.

2. Field experiment

a. Study site

All measurements were acquired in the Aulne estuary in Brittany, in northwestern France. The Aulne estuary is a shallow macrotidal tributary of the Bay of Brest. Its average discharge is $24\,m^3\,s^{-1}$, with a maximum in February ($75\,m^3\,s^{-1}$ monthly mean) and minimum in August ($3.5\,m^3\,s^{-1}$ monthly mean) (Allen et al. 1980), carrying approximately 7000 tons of suspended sediment in the Bay of Brest (Bassoullet 1979) each year. The estuary extends approximately 30 km upstream from its mouth, at the dam of Guily-Glaz, the latter stopping landward tidal propagation. The sediment bed in the estuary is characterized by a combination of sand and silty mud, with coarser material located downstream. In situ samples from Bassoullet (1979) reveal an evolving composition of

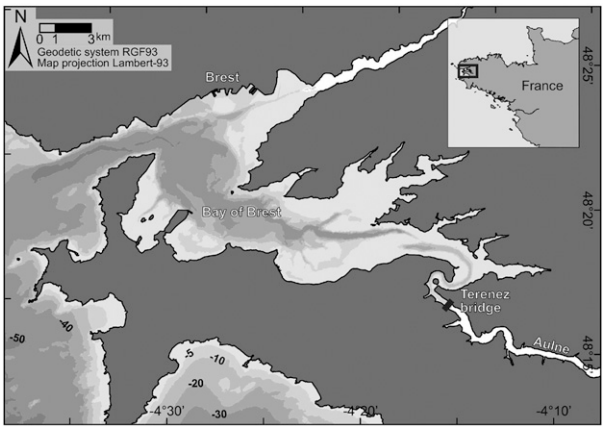

FIG. 1. Aulne estuary location. The Térénez bridge is located at the end of the estuary (48°16′07.38″N, 4°15′48.43″W).

the mud layer lying on the riverbed, with porosities from 0.65 to 0.9. The principal minerals in suspension have been identified as phyllitic clays, composed of illite, chlorite, kaolinite, and micas (Bassoullet 1979). The mass concentration of the suspended sediment varies seasonally, with the highest values observed in winter flood ($>1\,g\,L^{-1}$) and lowest in summer ($<30\,mg\,L^{-1}$). These fine-grained cohesive minerals are subject to the process of flocculation (Bassoullet 1979).

b. *Equipment and survey protocol*

Two similar 1-day experiments were conducted at a fixed location under the Térénez bridge in the Aulne estuary (Fig. 1) in 15 July 2014 and 21 January 2015. These 2 days correspond to two periods of spring tides—both having a tidal range of 8 m—but at low river discharge and at flood stage of the river, respectively. During more than 6 h of sampling during ebb, regularly spaced profiles of the water column were acquired with an Aquascat 1000S multifrequency profiler (Aquatec Group; Smerdon et al. 1998), a LISST-100X type C granulometer (Sequoia Inc.; Agrawal and Pottsmith 2000), and KOR-EXO1 multiparameter probe (YSI Inc.).

All instruments were attached horizontally to the same weighted downcast structure, ensuring consistency between the different measurements provided by the instruments. The instruments were first placed at a constant depth of 1–2 m to stabilize the sensors (especially the KOR-EXO multiparameter probe), before being brought to subsurface. Immediately after, the structure was downcast to the bottom at low speed, and upcast toward the surface.

The Aquascat 1000S measured the root-mean-square backscattered voltage V_{rms} at four frequencies (0.5, 1, 2, 4 MHz) on several cells in the horizontal direction at each ping. The length of the cells can vary from 2 to 40 mm. The Aquascat was set in the experiment to 5 mm for a total length of 1.28 m of measurements so that a total of 256 cells are recorded at each ping. The ping rate was set to 8 Hz and ensemble-averaged every eight pings before correcting for absorption, spherical spreading, and other system-dependent parameters (calibration constant, K_t). The measured acoustic backscatter values for each averaged ping resulted in an average of 100 horizontal sampling points centered around 0.5 m from the transducer, with a pulse length of 6.67 μs. The averaged sampled volume varied from approximately 1 cm^3 for the 4-MHz transducer (1.2° beamwidth) to 20 cm^3 for the 0.5-MHz transducer (4.85° beamwidth). The values for K_t were determined by the manufacturer in a water tank designed for that purpose.

The LISST-100X measured optical transmission, particle size distributions (PSD), and volume concentration. It is known to successfully determine the PSD of natural sediments and the size of monosized suspensions with 10% accuracy (Traykovski et al. 1999; Gartner et al. 2001; Gray and Gartner 2009) in the range 2.5–500 μm for type C instruments. The LISST-100X uses a 670-nm wavelength solid-state laser on a cylindrical volume of approximately 1.5 cm^3. The ping rate was set to 1 Hz, and each profile was initiated with a mechanical switch.

The YSI KOR-EXO1 multiparameter probes employ three sensors to record 1) salinity and temperature, 2) pressure, and 3) optical turbidity on single points. The ping rate was set to 1 Hz during the experiments.

In addition, in situ water samples were collected using a heavily weighted Niskin bottle at the same time intervals at a constant depth of 6 m (July) and 8 m (January). The uncertainty in the sampling depth was estimated at ± 0.5 m due to high discharge events for both experiments (spring tide conditions; current speed $> 1\,m\,s^{-1}$ during both experiments). Each sample was filtered using a 25 mm Millipore GF/F filter and weighted to determine the suspended sediment concentration (SSC). Turbidity data were further converted into SSC, thanks to the linear relationship existing between the water collected and the turbidity measured at the sampling depth, as shown in Fig. 2. The highlighted relationships appear to be independent of the time of year.

3. Preliminary observations

Probability density functions of the grain size distribution by volume were retrieved with the LISST-100X type C data in the range 2.5–500 μm (Agrawal and Pottsmith 2000; Gray and Gartner 2009). The optical inversion was performed using a kernel matrix designed for spherical particles (Agrawal and Pottsmith 2000;

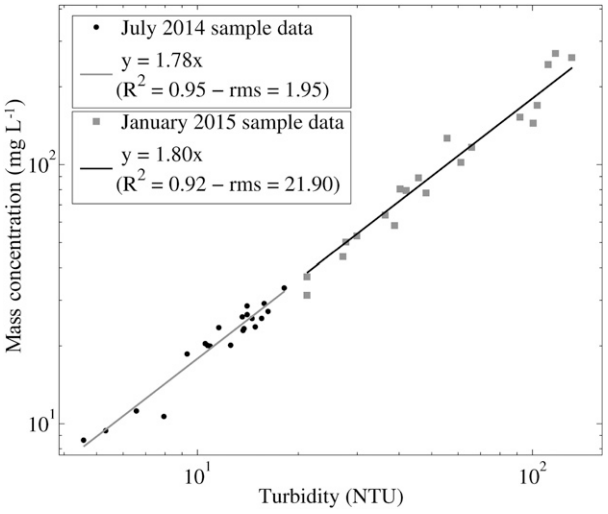

FIG. 2. Turbidity vs concentration relationship obtained from optical and in situ samples for the July 2014 and January 2015 experiments.

Andrews et al. 2010, 2011), which is used for general application to a wide range of natural particles. Sequoia Inc.'s MATLAB program was used to invert the LISST-100X data (Sequoia Inc. 2008). The data were systematically averaged every 0.5 m after processing. No interpolation was performed.

From one experiment to the other, the probability density function (PDF) by volume $v(a)$ seems to follow a lognormal distribution. The modes of the observed distributions are nearly constant during most of the ebb phase in July and during the first half of the ebb phase in January. Multimodal floc populations are observed close to the low water slack in July and during the second half of the ebb phase in January, characterized by a median diameter larger than 100 μm. In Fig. 3a it appears quite clear that most of the suspended material accounting for the total concentration is aggregated, forming small aggregates of diameters inferior to 100 μm. These particles will also be suspected to account for most of the backscattering observed with the ABS data. For the last four profiles of the July experiment, corresponding to the beginning of low tide slack water, and for several isolated profiles collected during the January experiment, exceptions occur as the shape of the distribution changes for the upper part of the water column, with higher volume concentrations observed in higher size bins (Fig. 3b). This phenomenon prevents the normalized standard deviation of the distribution to be found precisely, information required to compute the ensemble averaged backscattering properties of the suspension (Moate and Thorne 2009). However, it is possible to assert that the normalized standard deviation remained high (>0.7) for both experiments, indicating a broad size distribution of the suspended material.

Globally in January, LISST data are of lesser quality. Divergences appeared when the concentration exceeded ~150 mg L^{-1}, coupled with the ascension of the salinity gradient as the tidal level decreased, causing schlieren, which makes the results from the LISST untruthful (Styles 2006; Mikkelsen et al. 2008). The LISST was indeed not equipped with a path-reduction module to reduce the optical path in contexts of high turbidity. Bins where the mass concentration was higher than 150 mg L^{-1} and where the vertical salinity gradient exceeded 2 PSU m^{-1} were thus discarded from the analysis.

It is possible to estimate the mean effective density averaged over the total size distribution of the flocs ρ_{eff_m} using total volume concentration V_{tot} observed by the

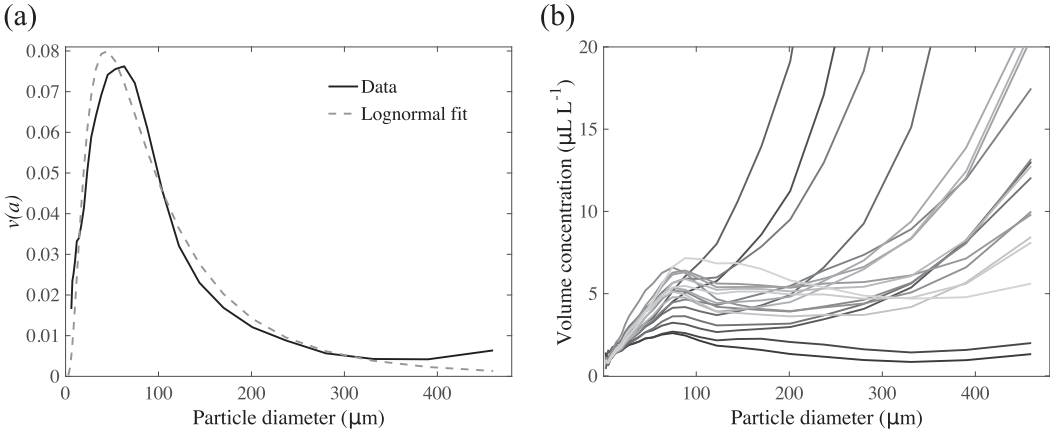

FIG. 3. (a) Lognormal fit (dashed line) to the PDF (solid line) by volume (January experiment, profile 8 at 6 m). (b) PDF by volume of profile 22 of the July experiment, showing the river surface (darker curves) down to the bottom (lighter curves).

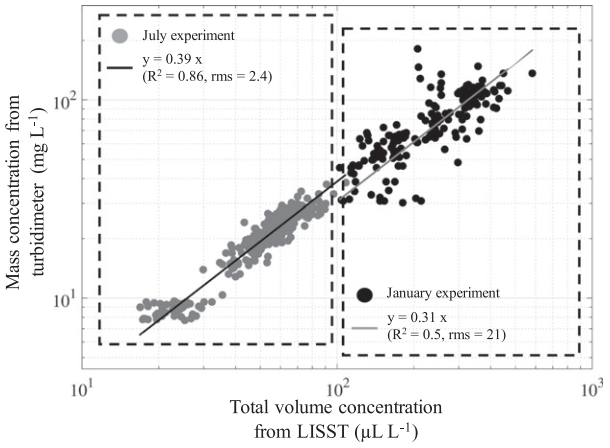

FIG. 4. Mean effective density estimation using optical turbidity converted into mass concentration according to the relations mentioned in Fig. 2 and the total volume concentration recorded by the LISST for the July (gray dots) and January (black dots) experiments. Some abnormal points of the total volume concentrations of the January experiments were discarded from the analysis.

LISST over its entire set of rings ($M \approx \rho_{\text{eff}_m} V_{\text{tot}}$). Figure 4 represents the output of this relation for the January and July experiments, revealing an effective density averaged over the total size distribution of ~300 and ~400 kg m^{-3}, respectively, which was nearly constant in both experiments. The trend is linear for both experiments, yet the data are more spread for the January experiment ($R^2 = 0.5$). These values are the result of several empirical relations (LISST calibration, spherical kernel matrix, water samples filtration and weighting, turbidity–concentration relationship), which bring high uncertainties (not estimated here) to the final result (Fettweis 2008). However, in view of these results, it is possible to assert that the mean effective density in January was lower than in July, and it seems to be constant during the whole experiments ($R^2 = 0.86$ in July, $R^2 = 0.5$ in January). This property, later qualified as ''apparent property,'' allows for considering a suspension of ''apparent particles'' of fixed mean porosity, the acoustic backscattering properties of which can be straightforwardly generated and can account for the whole suspension.

4. Scattering theory

In this section, the scattering theory associated with the current study is presented, in order to introduce the inverse model used to invert the collected ABS data and the employed inversion method.

a. *Backscattered signal*

For incoherent scattering from a suspension of particles, the V_{rms} recorded by a piston transducer can be written as follows (Thorne and Hanes 2002; Sheng and Hay 1988; Betteridge et al. 2008):

$$V_{\text{rms}} = \frac{K_s K_t}{\psi r} M^{1/2} e^{-2r(\alpha_w + \alpha_s)} \tag{1}$$

$$K_s = \frac{f}{(a_0 \rho_s)^{1/2}} \tag{2}$$

$$f_0(ka_0) = \left[\frac{\int_0^\infty an(a)\,da \int_0^\infty a^2 f(ka)^2 n(a)\,da}{\int_0^\infty a^3 n(a)\,da} \right]^{1/2} \tag{3}$$

In Eq. (1), M stands for the concentration of particles in suspension, r is the range, α_w is the attenuation due to water, α_s is the total attenuation due to the suspension, and ψ is the range modification factor (Thorne and Hanes 2002), taking into account the near-field correction. The quantity ρ_s is the density of the suspended material, k is the wave number, a is the particle radius distributed according to the number PDF $n(a)$, and a_0 is the mean particle radius. The quantity K_t here refers to a calibration constant determined for each transducer in a sediment suspension of known properties. The quantity K_s [Eq. (2)] refers to the scattering constant, depending on particle size, shape, and density. The term f is known as the form function and describes the backscattering characteristics of the suspension; its expression can be found analytically by resolving the wave equation considering simplistic shapes (spheres, cylinders, etc.), and consists of a summation of an infinite number of vibrational scattering modes. For the present study, a model was designated to describe the intrinsic backscattering properties of a spherical particle, built as a high-pass solution (Johnson 1977) and designed in order to take into account the fluidlike properties of apparent particles of low density.

For marine sediments, in particular noncohesive sand, Hay (1991) and later Thorne et al. (1993) used a heuristic approach based on Sheng and Hay (1988) to elaborate an expression of the backscattering form function, entirely defined by the density and compressibility contrasts between the particle and the medium. For fluidlike particles, Thorne et al. (2014) reemployed the general shape of this particular backscattering form function with a Rayleigh regime entirely defined by the acoustic impedance contrasts between the particles and the medium, but with a lower convergence in the geometric regime, accounting for the enhanced penetrability of the object. Moreover, no oscillation terms are added in the final shape of the form function as for solid particles (Thorne et al. 2014). The form function for fluidlike particles is given as follows:

$$f = \frac{K_f (ka)^2}{1 + \varepsilon (ka)^2}, \tag{4}$$

$$K_f = \frac{2}{3}\left(\frac{\gamma\zeta^2 - 1}{3\gamma\zeta^2} + \frac{\gamma - 1}{2\gamma + 1}\right), \tag{5}$$

$$\gamma = \frac{\rho_f}{\rho_w}, \quad \text{and} \quad \zeta = \frac{c_f}{c_w},$$

with γ and ζ being the ratios of density ρ and sound velocity c between the particle and the water, respectively. The subscript f refers to the fluidlike properties and the subscript w to the water. The ε is a constant set to take into account the penetrability of the particle in the geometric regime (Stanton 1989). Thorne et al. (2014) set this constant equal to 1.2–1.4 but also mention a certain degree of uncertainty due to a lack of laboratory measurements. Instead of setting this value to a pragmatically selected constant, the ε parameter was determined in the present study as a function of the Rayleigh coefficient R_f, by computing the second-order high-pass filter with regard to the Rayleigh and geometric limits of the model as:

$$\varepsilon = \frac{K_f \sqrt{2}}{2R_f}, \tag{6}$$

$$R_f = \frac{\gamma\zeta - 1}{\gamma\zeta + 1}.$$

b. *Apparent particle scattering model*

MacDonald et al. (2013) showed that neither an elastic sphere nor a fluid sphere model correspond to the response of a suspension of flocculated sediments (kaolin). Yet, somehow the backscatter response of the suspension was located in between the predicted response from the elastic and fluid sphere models, and showed similarities with the heuristic expression of Moate and Thorne (2009). Indeed, the aggregates can be seen as a matrix of several primary particles linked together but filled with interstitial water, leading to lower density and sound velocity (compressional and shear waves) when considering the aggregate as a whole (Thorne et al. 2014). Regarding these conclusions, it seems unavoidable to take into account both the fluid and solid contributions of the aggregated particles. The problem resides in how to express these contributions in a backscattering model. All published works seem to agree with the idea of considering some kind of weighted solid–fluid particle in the Rayleigh regime (Sheng and Hay 1988; MacDonald et al. 2013; Thorne et al. 2014). To some extent, these particles can be locally assimilated into porous unconsolidated granular material, the water and solid components each contributing to the bulk compressibility and bulk density of the floc.

Considering an unconsolidated sediment layer of porosity Φ, the bulk density ρ_0, and the bulk modulus κ_0 of the medium can be defined as follows (Wood 1964):

$$\begin{cases} \rho_0 = \Phi\rho_w + (1 - \Phi)\rho_s \\ \dfrac{1}{\kappa_0} = \dfrac{\Phi}{\kappa_w} + \dfrac{(1 - \Phi)}{\kappa_s} \end{cases} \tag{7}$$

$$c_0 = \left(\frac{\kappa_0}{\rho_0}\right)^{1/2}, \tag{8}$$

where ρ_w and ρ_s are the densities of the porous water and the sediment grains, respectively. The κ_w and κ_s are the compressibilities of the porous water and the sediment grains, respectively. Here, ρ_0 and κ_0 may be interpreted as weighted means of the respective values for the two materials. The c_0 is Wood's sound speed (Wood 1964). The calculation of Wood's sound speed in this case supposes that no shearing occurs.

Modifying Eqs. (4)–(6) by adding the effects of the bulk compressibility and bulk density [Eqs. (7) and (8)] leads to reducing the impedance contrast between the particle and the medium. Such a model describes the scattering characteristics of an apparent suspension of monosized spherical particles, the porosity of which does not vary with size (Fig. 5). Such apparent particles are not to be understood as physical particles, but as particles that describe an averaged behavior of the suspension (mean porosity) over the physical size distribution. No physical information in terms of particle size can be extracted from this approach. However, this kind of representation can reveal itself of practical use to tackle the exposed problem (and retrieve the SSC), at least for a limited range of sizes (by definition, primary particles will not have reduced densities) and by extension for a limited range of ka values. Further in this study, the model will be limited to ka values located before the geometric region ($ka < 2$), for which the directivity of the suspended elements might play an important role in the backscattered signal.

This model in fact corresponds to the case where the same mean porosity is applied for all sizes in the Thorne et al. (2014) model. Indeed, Thorne et al. (2014) considered the property of the aggregated particles to see their effective densities vary according to their size as follows:

$$\gamma(a) = 1 + \frac{C_f}{a^m \rho_w} \tag{9}$$

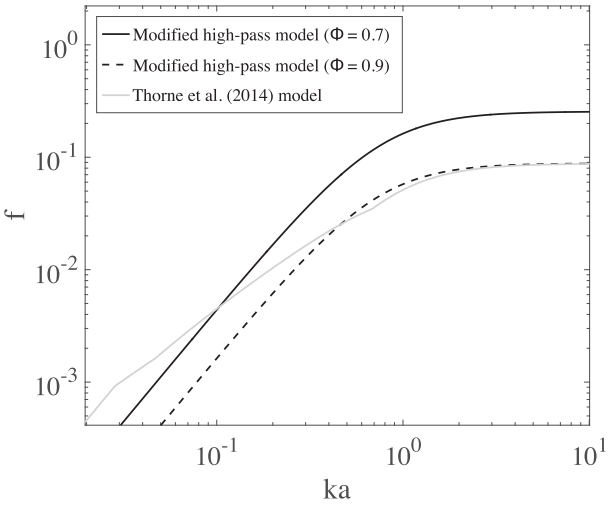

FIG. 5. Illustration of the model used to invert the backscattered signal from the aggregated particles in suspension (black lines). The Φ is the porosity chosen as input for the backscattering model: 0.7 (solid line) and 0.9 (dashed line). The gray line corresponds to the Thorne et al. (2014) model. Parameters necessary to compute the model are as follows: $C_f = 1 \times 10^{-3}$ kg m$^{3\text{-}m}$, $m = 1.1$, $\gamma_0 = \zeta_0 = 1.05$, $\rho_s = 2650$ kg m^{-3}, $\rho_w = 1000$ kg m^{-3}, $c_s = 5500$ m s^{-1}, $c_w = 1480$ m s^{-1}, and $\varepsilon_1 = 1.4$.

$$\zeta(a) = \frac{1}{c_w}\left\{\left[\frac{\Phi}{\rho_w c_w^2} + \frac{(1-\Phi)}{\rho_s c_s^2}\right][\Phi\rho_w + (1-\Phi)\rho_s]\right\}^{(-1/2)}. \tag{10}$$

Here c_w and c_s are the sound velocity in the water and in the primary particles constituting the aggregates, respectively; and ρ_w and ρ_s are the densities of the water and the primary particles constituting the aggregates, respectively. The values of C_f and m vary depending on the process of flocculation (Thorne et al. 2014). This model also needs to be constrained by the addition of a minimum ratio of velocity ζ_0 and density γ_0, thus bounding the minimum density and sound velocity in the aggregates. No generic table exist to fix these parameters according to in situ conditions, which makes this model difficult to apply to real data.

In this article, no assumptions about the sediment attenuation were made. Knowing exactly the influence of the viscous and scattering contributions of the total sediment absorption for such particles is intricate in practice (MacDonald et al. 2013). During our experiments, the acoustic signal strength recorded along the horizontal profiles remained steady after beam spreading and water absorption corrections. This suggests that the total absorption due to sediment was negligible, or at least remained sufficiently low due to the short distance investigated (1 m), despite some moderate turbidity events. Thus, in this study, it appears reasonable to suppose that the total attenuation due to sediment was negligible, as this was observed with in situ ABS profiles at each frequency for the highest concentrations.

c. Inversion method

Different notations exist in the literature to describe the backscattering characteristics of a particle (Sheng and Hay 1988; Stanton 1989; Thorne and Hanes 2002). More precisely, Medwin and Clay (1997) express the relation between the form function described in Eq. (4) and the backscattering cross section σ_{bs} of Eq. (11) as follows:

$$\sigma_{bs} = \left(\frac{af}{2}\right)^2. \tag{11}$$

With concern for naming conventions, the use of the volume backscattering coefficients as described by Maclennan et al. (2002) rather than V_{rms} was preferred. Using Eqs. (1) and (11), the volume backscattering strength S_v and volume backscattering coefficient s_v can be written as follows:

$$\begin{aligned} s_v &= N\sigma_{bs} = \frac{3}{\pi}\frac{V_{rms}^2 \psi^2 r^2}{16K_t^2} e^{4r(\alpha_w+\alpha_s)} \\ M &\approx \frac{N\rho_f 4\pi}{3}\int_0^\infty a^3 n(a)\, da \\ S_v &= 10\log_{10}(s_v), \end{aligned} \tag{12}$$

where N [Eq. (12)] refers to the number of particles per unit volume. The attenuation due to water was calculated according to the Francois and Garrison (1982) model. The sound speed in water calculation was performed using the Chen and Millero (1977) formula. Attenuation due to sediments was neglected in this context. Once converted into s_v values, the data were averaged over 100 sampling points per depth (as each ping of the instrument insonified the water column horizontally) so that a complete profile is obtained with one s_v value per frequency per depth. Then the data were averaged over 0.5-m vertical bins. Every s_v measurement is thus the average of at least 800 values (for a corresponding downcast speed between 0.25 and 0.5 m s^{-1}). The volume backscattering coefficients obtained for each depth were then inverted following the nonnegative least squares (NNLS) method. The NNLS method has been employed and validated before in a similar context of multifrequency acoustical inversion and is well documented in the literature (Lawson and Hanson 1974; Greenlaw and Johnson 1983; Holliday and Pieper 1995; Hwang et al. 2007). The concept rests upon considering that the measured s_v is

the linear combination of the individual contributions of the particles present in the sampled volume,

$$s_v(\nu) = \sum_i \sigma_{\mathrm{bs}}(a_i, \nu) \times N_i, \tag{13}$$

where a_i is the equivalent spherical radius (ESR), ν is the frequency, and N_i is the abundance (or number of particles per unit volume) of particles with an ESR a_i.

The unknown of the inverse problem is N_i [Eq. (13)] with an ESR a_i. As input, the algorithm needs a vector of mean volume backscattering coefficients measured at all used frequencies, and the user must choose a size vector indicating the n assumed equivalent sizes of the occurring particles. In practice, the number of sizes of interest must not be larger than 4 times the number of frequencies (Greenlaw 1979; Lebourges-Dhaussy 1996). The number of size classes was thus chosen equal to 16, against four frequency observations, hence the underdetermined nature of the present inversion. The present model (contained in σ_{bs}) was computed for each input size a_i and measured frequency ν_j. It is implemented as its intrinsic form, that is, without being ensemble averaged over the size distribution. Equation (13) can be written as the matrix system below, after normalizing by s_v and adding a damping parameter λ, according to the Levenberg–Marquardt analysis method (Lawson and Hanson 1974), to overcome underdetermination issues and to constrain the choice of the solution. The λ was set to 10^{-6}, assuring that the norms of the solution and the associated residual error are minimal (Lawson and Hanson 1974; Greenlaw 1979). The algorithm is based on an iterative process that evaluates the residual errors E [Eq. (15)] to further estimate a better solution, with a constraint of nonnegativity on the solution. Successive inversions are performed until the residual error is close to a minimum,

$$\begin{pmatrix} \dfrac{\sigma_{\mathrm{bs}}(a_i, \nu_j)}{s_v(\nu_j)} \\ \mathbf{I}(n) \times \|\mathbf{A}\| \times \lambda \end{pmatrix} \times \mathbf{N} = (1 \ldots 10 \ldots 0)^{\mathrm{T}} \tag{14}$$

$$\mathbf{A} = \left[\frac{\sigma_{\mathrm{bs}}(a_i, \nu_j)}{s_v(\nu_j)} \right]$$

$$E = \left\| \frac{\sigma_{\mathrm{bs}}(a_i, \nu_j) \times \mathbf{N} - s_v(\nu_j)}{s_v(\nu_j)} \right\|. \tag{15}$$

Here, $\mathbf{I}(n)$ is the identity matrix of size n × n, and the $\| \, . \, \|$ stands for the operator norm. The N_i abundances from vector $\mathbf{N}$ associated with the equivalent spherical radii a_i can be further converted into equivalent sphere volumes in order to obtain a volume concentration, and if the density of the particles is known, into a mass concentration [$M_i = \rho_0 N_i (4/3)\pi a_i^3$].

When using this kind of acoustic inversion method, particular attention has to be paid to the choice of the size vector. The combination of measured frequencies and size classes chosen as input, or the parameter ka, has to cover the transition region between Rayleigh and geometric scattering so that the elements of the inversion matrix $\mathbf{A}$ [Eq. (14)] can be linearly independent (Greenlaw 1979; Lebourges-Dhaussy 1996). In this study, using frequencies ranging from 0.5 to 4 MHz, the minimum size to choose in order to avoid such problems is close to 30 μm ($ka > 0.5$), assuring that the elements of the matrix are linearly independent. To the contrary, the larger size chosen was set to 500 μm, assuring that the model will not span the geometric region, which is uncertain in this context. As there were few chances to observe large-sized particles–flocs (only one event of high flocculation occurred during the first experiment in July 2014), the latter vector was logarithmically spaced to better represent the sizes of interest.

5. Results

a. Physical parameters

Figure 6 shows the evolution of median diameters D50 (calculated from the LISST data), salinity, temperature, and SSC profiles during the whole experiments (July 2014 and January 2015). The origin of the graphs is taken at the surface. The time lapses between each profile are about 15 min for both experiments. For the January experiment, the first profiles (1–10) were delicate to achieve due to the presence of a strong current preventing the downcasting structure from reaching the bottom of the river. Only half of the water column could be sampled then. More generally, a specific attention was paid to the immersion depth of the downcasting structure in order to avoid touching the bottom of the river, thus leaving a gap of at least 1–2 m between the structure and the bottom.

The vertical structure of the water column is quite different from one experiment to the other. The July experiment is characterized by a temporal salinity gradient but a mixed water column, the freshwater from the river slowly taking the upper hand on the saltwater from the sea (ebb context). To the contrary, in January a strong vertical salinity gradient is observed. Its position in the water column evolves with the tide, nearly reaching the surface at the end of the experiment. The temperature variations of both experiments are quite

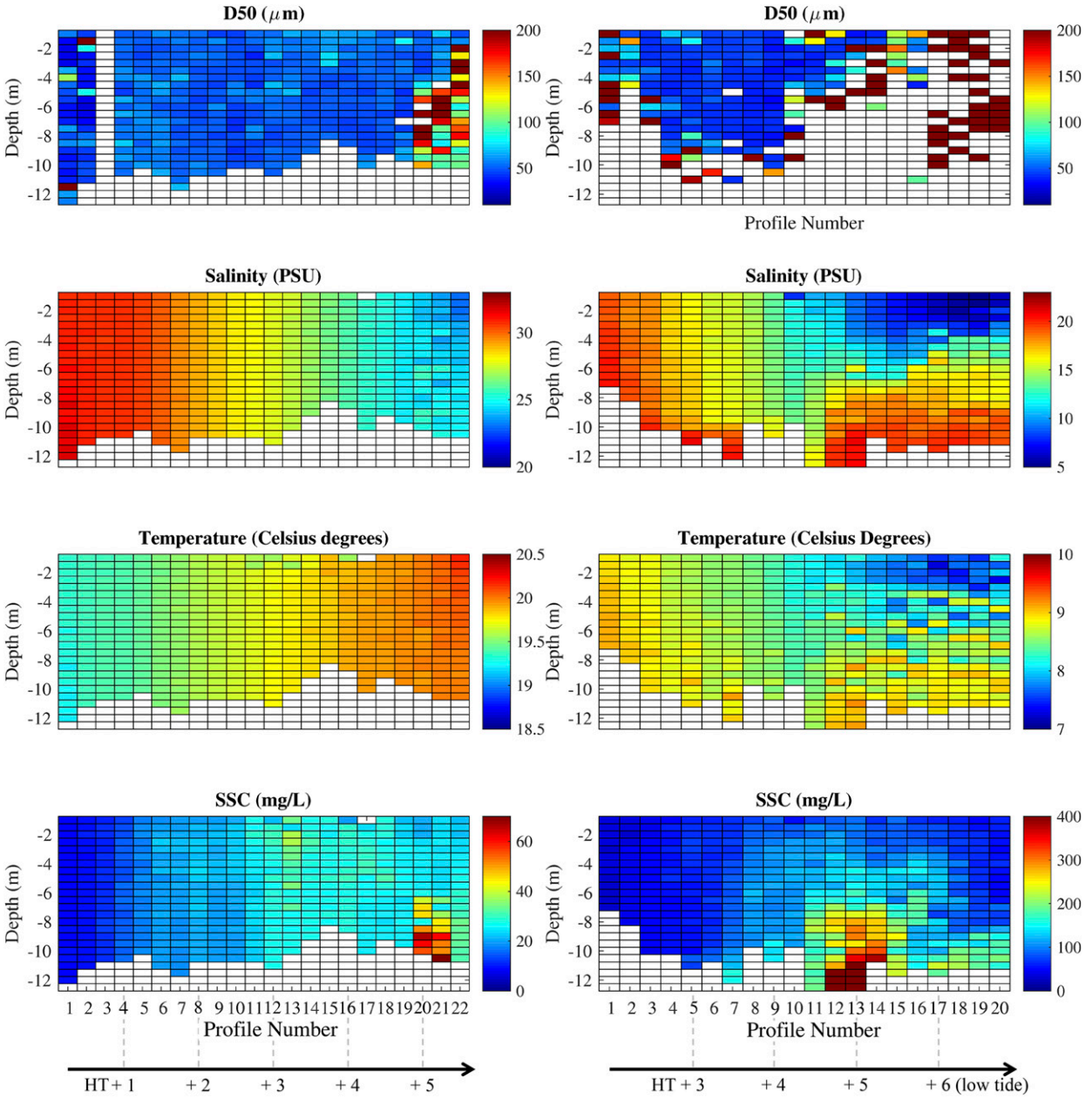

FIG. 6. Physical parameter variations for the (left) July and (right) January experiments. (top to bottom) D50 (μm), salinity (psu), temperature (°C), and SSC (mg L^{-1}). The black horizontal arrows below both columns indicate the tide time (h) after high tide (HT). The reference is taken at the water surface.

limited in amplitude, with an increase from 19° to 20° observed in July and a decrease from 9° to 7.5° in January. A small temperature gradient appears at the end of the January experiment due to the presence of unmixed freshwater coming from the river at slack tide. The recorded turbidities, here converted to SSC thanks to the relation found Fig. 2, are highly different between July and January. The former is characterized by a slow evolution throughout the experiment (15–90 mg L^{-1}), with no variation recorded on the vertical except around low tide (profiles 19–22). The latter is characterized by a moderate turbidity event localized in time and depth between profiles 7 and 18 (30–550 mg L^{-1}). Salinity and temperature values were used to compute the water density throughout the experiments, as well as the speed of sound. The latter varied from 1515 to 1509 m s^{-1} during the July experiment, and from 1470 to 1450 m s^{-1} during the January experiment.

D50 remain rather steady for most of the July experiment (profiles 1–18), with values scattered around 50 μm. No data were recorded during profile 3 (the mechanical switch was in the "off" position). For the last three profiles, the D50 values are higher, scattered around 150–200 μm (Fig. 3b). This part of the experiment appears to be subjected to more intense flocculation.

Concerning the January experiment, the data are of lesser quality. Bins with high SSC and salinity gradient were discarded (see section 3), leaving around half of the dataset. Moreover, the processing routine sometimes experienced difficulties attributing values of volume concentration, especially in the lower part of the water column ("Not a Number" values attributed instead). Nevertheless, for the first half of the experiment (profiles 1–11), the D50 values are stable, scattered around 40 μm. After profile 11 (the transition from ebb to low slack), the D50 values seem to follow the same trend as for the last three profiles of the July experiment, with higher values reaching up to 300 μm. The LISST data were not used as input to the acoustic inversion. As exposed in section 3, they mostly served the purpose of highlighting the steadiness of the mean effective density throughout the experiments.

b. *Inversion outputs*

To proceed with the acoustic inversion, the eventual parameters to be determined are the density of the elementary particles and an estimate of the porosity of the aggregates. Those parameters will particularly impact the intrinsic scattering properties of the suspension, preventing the multifrequency inversion from reaching a high degree of accuracy. Bassoullet (1979) described the riverbed of the Aulne as a muddy environment composed of phyllitic clay. Usually, the particle density of normal soils is around 2650 kg m^{-3}. This value will be used for the following inversion. Correspondingly, the sound speed in the primary particles was chosen equal to $c_s = 3400\,\mathrm{m\,s^{-1}}$ (Castagna et al. 1985; Han et al. 1986) but revealed itself not to be of significant importance in the final result (given a fixed high $\Phi = 0.85$ and a change in sound speed velocity in the primary particles $\Delta c_s = 100\,\mathrm{m\,s^{-1}}$, the resulting change in sound speed velocity of the aggregated material Δc_0 is $<0.1\,\mathrm{m\,s^{-1}}$).

As observed in the LISST data (Fig. 4), the assumption of a fixed mean porosity is introduced in the model as input for the inversion. For each experiment, an optimal porosity (for which the best fit is observed between the mass concentration estimated by acoustics and the in situ measurements) was thus determined for the model exposed.

In parallel, the porosities of the Aulne surface sediment are exposed in Khalil et al. (2013) at three different stations along the estuary, for February, May, July, and October 2009. These values (Table 1 in Khalil et al. 2013) are used as reference to compare the actual values of porosities inserted in the inversion. Khalil et al. (2013) indicate a porosity of the surface sediment near the Térénez bridge of $\Phi = 0.9$ for their February sampling (i.e., corresponding to apparent particles with a density of $\sim$1180 kg m^{-3}). This value is closest to the January experiment, characterized by a high river discharge. Such a high porosity can be explained by the occurrence of strong currents tending to increase the soil erodibility, thus leaving a highly porous water–sediment interface covering the riverbed. Similarly, Khalil et al. (2013) indicate a porosity around 0.8 in July 2009 near Térénez bridge (corresponding to apparent particles with a density of $\sim$1340 kg m^{-3}). These values are susceptible to change according to the environmental conditions (measurements collected in 2009) as well as along the river and during the experiment (Khalil et al. 2013), but they offer a consistent order of magnitude of what could occur in the suspension of flocculated sediments. In addition, the collected measurements in 2009 indicate that the general trend of surface sediment porosity is seasonal, with higher porosity values in winter and lower in summer. This general trend can also be observed with the effective densities estimated from the LISST (Fig. 4). A higher porosity is a priori expected for the January experiment. For each profile, the mean velocity of the sound in the water and the mean density of the water were added to the inversion to take effect on the apparent particle density and speed of sound calculation.

For what concerns the January experiment, the optimum porosity value for the present model appeared to be 0.87 (i.e., effective density of $\sim$213 kg m^{-3} for a mean density of water of 1015 kg m^{-3}), whereas the one for July was estimated to be 0.85 (i.e., effective density $\sim$244 kg m^{-3} for a density of water of 1025 kg m^{-3}). These values depend entirely on the primary particle density chosen previously and would be different for different densities. The corresponding values for γ and ζ were close to 1.2 and 1, respectively. The following section presents the results in terms of total mass concentration and equivalent spherical radii solutions.

1) TOTAL MASS CONCENTRATION

Figures 7 and 8 display the results of the inversion for the July and January experiments, respectively. Both results were obtained by summing the solution over all size classes of ESR chosen as input for the inversion. The inversion outputs show reasonable results, in good agreement with the actual in situ concentrations

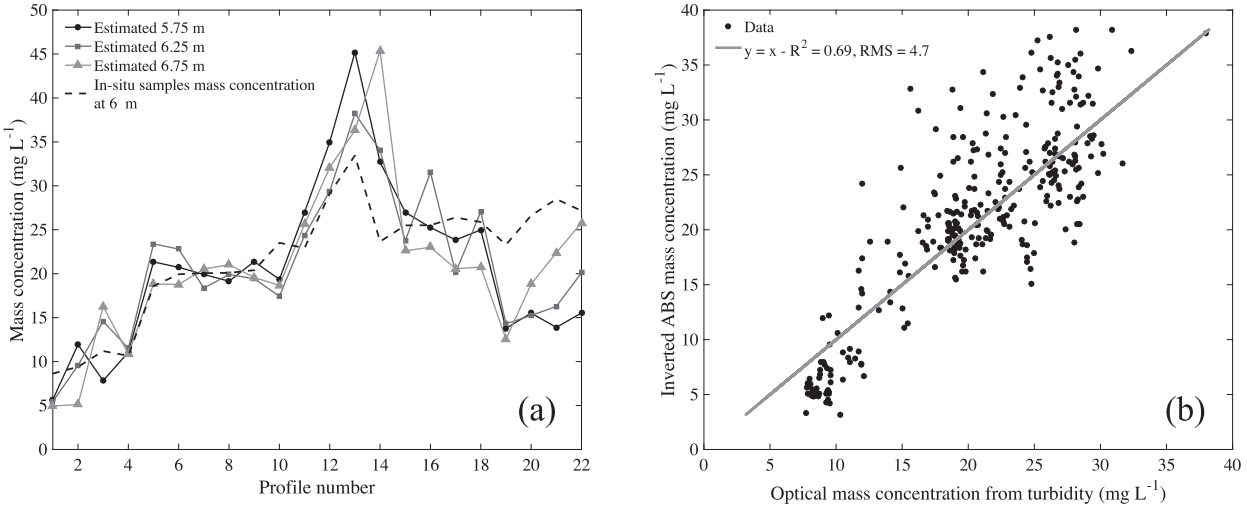

FIG. 7. (a) Output of the inversions using the modified high-pass model for the July experiment at different sampling depths: 5.75 m (circles), 6.25 m (squares), and 6.75 m (triangles). (b) Overall comparison between the optical turbidity converted into mass concentration (Fig. 3) and inverted mass concentration.

estimated thanks to the calibrated turbidimeter—yet are more spread as the concentration increases. The global variations of the total suspended sediment mass concentration are well reproduced by the inversions of both experiments, this for both low and high suspended loads.

Concerning the July experiment, Fig. 7a compares the mass concentrations obtained with the water samples to the output mass concentration found around the sampling depth. Except for the last four profiles, the results are consistent, as both concentrations follow the same variations throughout the experiment in spite of the high natural variability of the medium. The poor range of mass concentrations experienced is certainly at the origin of the lower correlation coefficients ($R^2 = 0.69$; Fig. 7b); however, a clear linear trend can be drawn on the graph. Moreover, below 10–15 mg L^{-1} the algorithm underestimates the actual concentration, most certainly due to a low signal-to-noise ratio.

The range of mass concentrations experienced during the January experiment is wider, from 50 to 800 mg L^{-1}. The correlations are higher ($R^2 = 0.77$; Fig. 8b) even if a localized overestimation of the concentrations by the acoustic inversion seem to appear after profile 11 (Fig. 8a). Moreover, these deviations can be reduced when averaged around the sampling depth, although they seem to indicate a small change in the aggregates

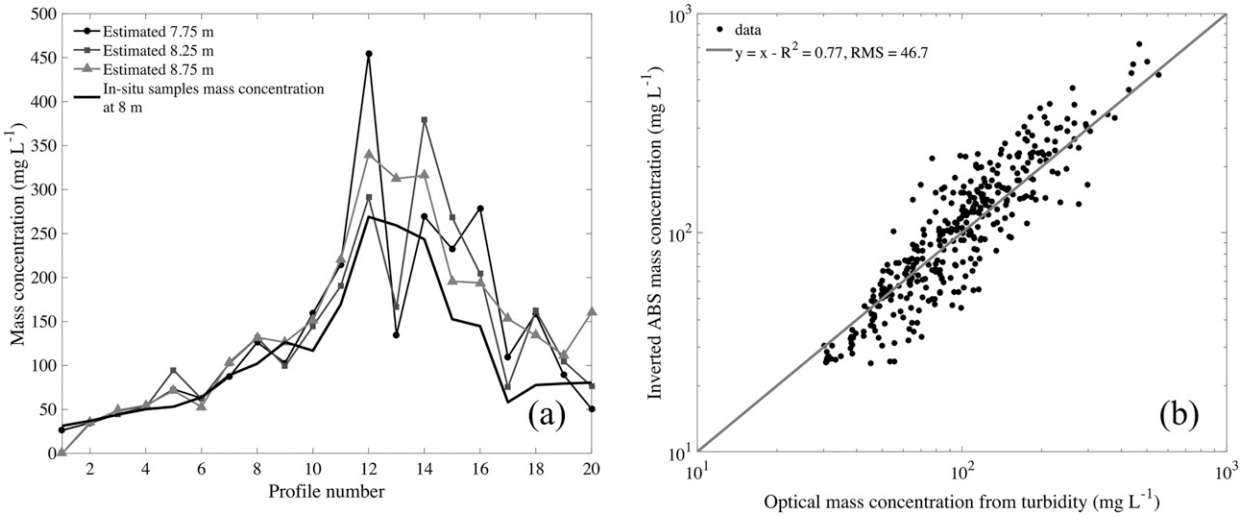

FIG. 8. As in Fig. 7, but for the January and sampling depths of: 7.75 m (circles), 8.25 m (squares), and 8.75 m (triangles).

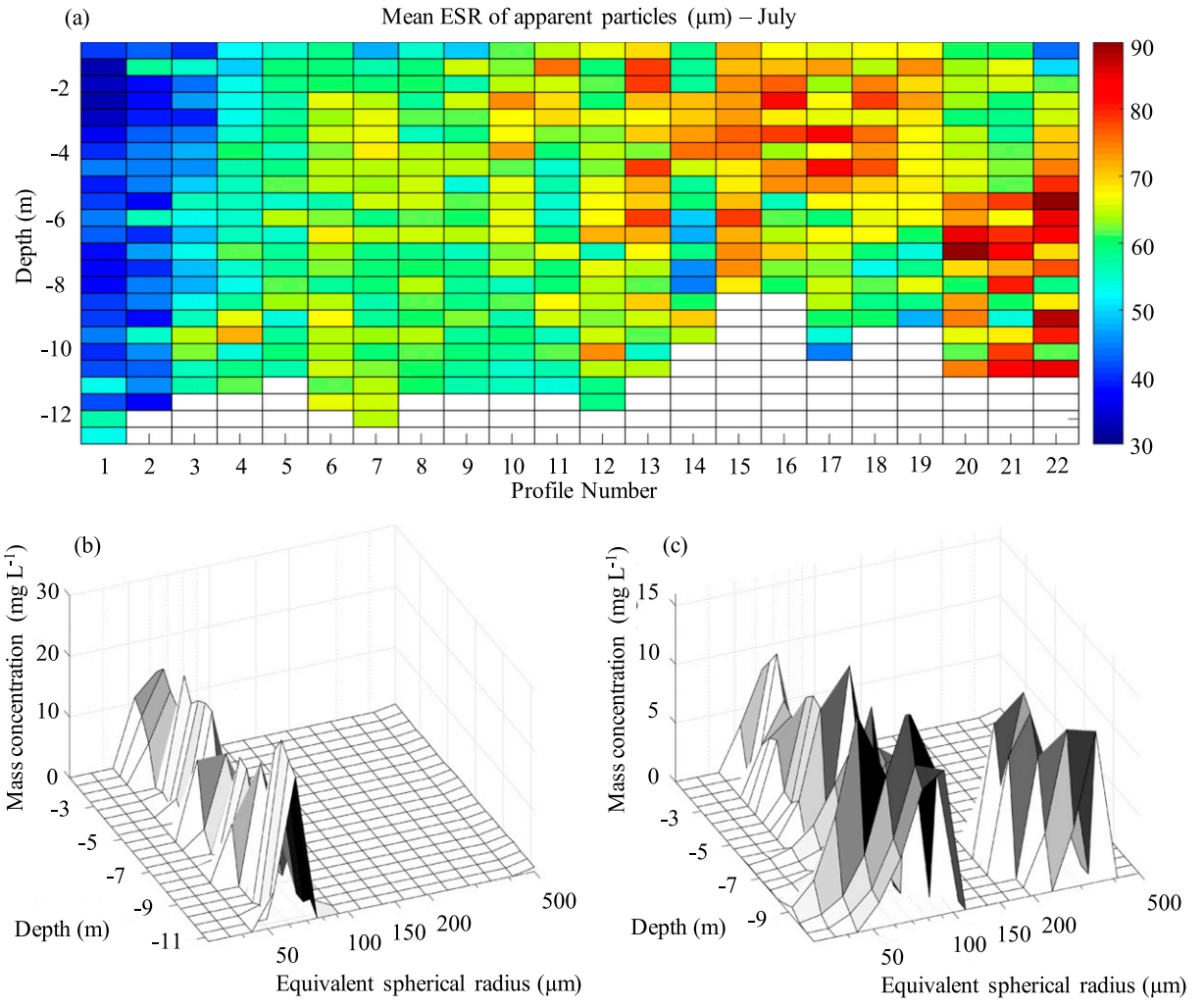

FIG. 9. (a) Mean equivalent spherical radii calculated from the abundance solution of the inversion for the entire July experiment. These are the radii of apparent particles accounting for the suspension backscattering properties. NNLS output results for (b) profile 6 and (c) profile 20 of the July experiment. Both are displayed as a function of depth (m), ESR (μm), and attributed mass concentration (mg L^{-1}). For (b), one dominant mode is found to dominate the scattering. For (c), the solution is mainly allocated to two distinct modes of ESR beyond 7 m.

physical properties, to be linked with the vertical salinity gradient.

2) EQUIVALENT SPHERICAL RADIUS

It is worth reminding that the size values in which a solution has been attributed by the NNLS algorithm do not correspond to the physical radii of the suspended particles. Their interpretation must remain qualitative, as the presented approach focuses on the apparent particles of fixed porosity, used to describe the acoustic behavior of the suspension.

Figures 9a and 10a illustrate the mean radii of the apparent particles considered in this paper for the July and January experiments, respectively. The mean radii were calculated from the abundance distribution, without any knowledge of the inverse problem [Eq. (14)]. During the July experiment, the mean radii steadily increase from 35 μm at profiles 1–2 to 70–80 μm at profiles 17 and 18. Rather than a vertical stratification, slight inhomogeneities appear on the vertical, which is also the case for D50 values (Fig. 6). However, the final result converted to mass concentration is not biased by this variability and remains stable (Holliday and Pieper 1995). The last three profiles of the experiment are characterized by a clear vertical stratification where larger particles ($a > 80\,\mu$m) occupy the last part of the water column, from 6 to 12 m. These observations are in agreement with the LISST D50 (Fig. 6).

The January experiment exhibits a rather different behavior. The water column seems homogeneous in

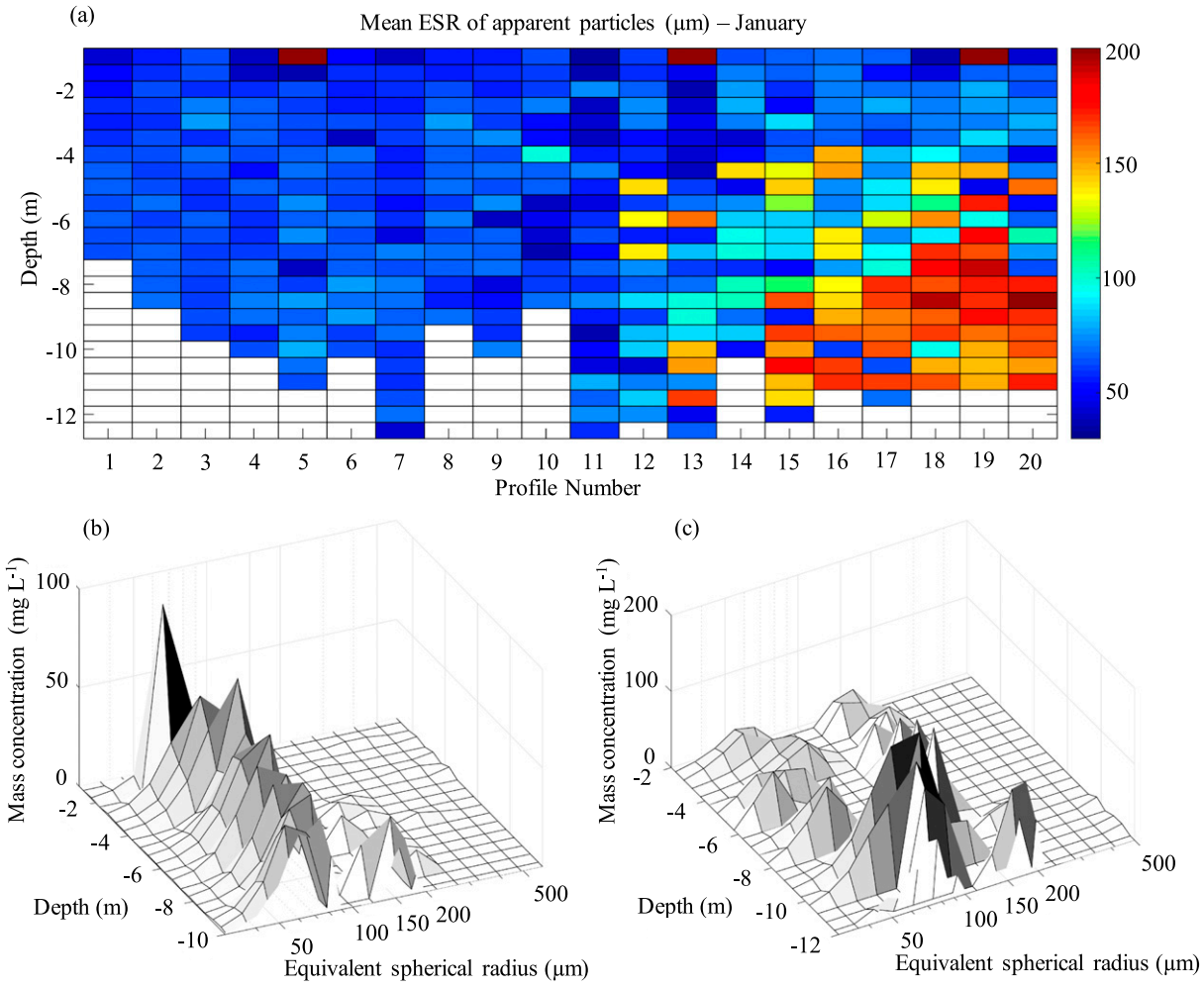

FIG. 10. As in Fig. 9, but for the January experiment and for (b) profile 8 and (c) profile 12. For (c), the solution is mainly allocated to two distinct modes of ESR.

terms of mean ESR from profiles 1 to 11, with mean radii values close to 45 μm. From profile 12 onward, a clear stratification following the salinity vertical structure (Fig. 6) can be clearly identified, below which mean radii can reach values up to 200 μm. Vertical variability is also observed at this point.

For what concerns most of the July experiment (profiles 1–18) and the first half of the January experiment (profiles 1–11), the solution of the inversion is attributed to a dominant size mode of ESR, around which a smaller solution is allocated to neighboring modes (Figs. 9b and 10b). The dominant mode is (in terms of mass concentration) between 35 and 60 μm for the July experiment (Fig. 9b) and 60–90 μm for the January experiment (Fig. 10b).

During the July experiment, a second dominant mode appears after profile 18 in the lower part of the water column (Fig. 9c), beyond 7 m, centered around 235 μm. Similarly, starting at profile 11 of the January experiment, a second dominant mode appears around 135–165 μm in the lower half of the water column (Fig. 10c). These examples correspond to the beginning of low tide slack water (Fig. 6), where misfits appear in terms of mass concentration (Figs. 7 and 8). These discrepancies result in a factor of 1.5–2 in terms of final mass concentration estimate during the July experiment (Fig. 7a) and ~1.5 during the January experiment (Fig. 7b). A change in the hydrodynamics conditions, influencing the aggregation process seems plausible at this stage, and bigger aggregates are likely to be formed due to a lower shear rate (Verney et al. 2011) and salinity gradients. The allocation of the solution into several dominant ESR may be responsible for the misfits in terms of mass concentration, especially for the higher size classes, where a small modification in the numerical density has a heavy influence on the final volume concentration.

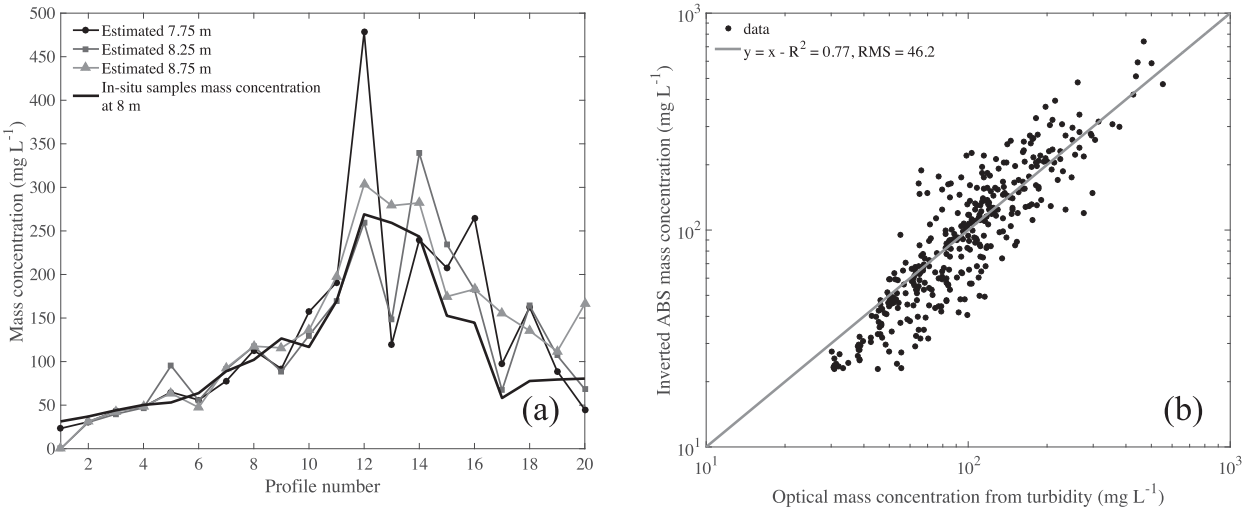

FIG. 11. As in Fig. 8, but using the Thorne et al. (2014) model for the January experiment.

3) COMPARISON WITH THORNE ET AL. (2014) MODEL

The Thorne et al. (2014) model was used to invert the present datasets. However, a certain number of parameters had to be chosen arbitrarily, in the ranges suggested by the same authors. Several sets of parameters may exist. The inversion results in terms of total mass concentration are presented in Fig. 11 for the January experiment, with the following parameters chosen as input for the model generation: ρ_s = 2650 kg m^{-3}, c_s = 5500 m s^{-1}, ε_1 = 1.4, C_f = kg m^{-3}, 1.1 m, γ_0 = 1.09 , and ζ_0 = 1.05. The quantities C_f and m are extremely delicate to estimate in situ, and this would have required precisely measuring the aggregates' settling velocity and size. Their values were chosen by default after Thorne et al. (2014). For the ESR spectrum used in this study, setting γ_0 to 1.09 had a threshold effect on the effective density, fixing the latter at 90 kg m^{-3} for all sizes. Thus, this model is very close to the one exposed here, yet converging toward a lower limit. In this case ε is set to 1.4—instead of a value close to 1.8 (in July) and 1.9 (in January) in the model designed in this paper—this ε parameter being a function of the penetrability of the apparent particle, hence the lower mean effective density for the Thorne et al. (2014) model.

The retrieved mass concentrations are consistent with those obtained thanks to the calibrated turbidimeter (Fig. 11b). The exact same trend can be observed between the two models (Figs. 8 and 9), with a high correlation (R^2 = 0.77) for the entire dataset.

The ESR modes identified by the algorithm (not shown here) are also close to those found by the presented model. As mentioned above, both models possess closed shapes in the *ka* region of interest, as the effective density is somehow fixed in the Thorne et al. (2014) model; therefore, they vary accordingly.

6. Discussion

a. General comments

In this paper, a model was designed that takes into account aggregated particles, assuming they can be approximated by apparent particles of fixed low density. Its Rayleigh regime increases according to $(ka)^6$, the level of which depends on the ratios of density and compressibility. Beyond the transition region around ka = 1, the model converges toward a high-pass limit, a function of the penetrability of the object. Consequently, the aggregated particles are in fact considered weakly scattering bodies, as it is the case for several species of zooplankton (Stanton et al. 1998). This representation of the suspension, made of (conceptual) apparent particles of low density, is far from the traditional ways of accounting for the backscattering properties of suspended sediments. Yet, it has the main advantage of freeing oneself from the large uncertainties that exist in the flocculation process, which is delicate to evaluate in in situ studies.

To proceed with the inversion of the acoustic measurements, the NNLS method was chosen over traditional implicit methods used in suspended sediment dynamics studies (Thorne and Hardcastle 1997; Thorne and Hanes 2002). This method is commonly used when solving multifrequency inverse problems in halieutics (Lawson et al. 2008; Cox et al. 2013; Lebourges-Dhaussy

et al. 2014), but it has never been addressed in suspended-sediment-related studies. Its use was motivated here by the difficulties encountered in estimating the distribution width, preventing the ensemble averaging of the form function (Moate and Thorne 2009). Similarly, the use of quantities, such as S_v instead of V_{rms} in the problem statement, was preferred due to its major involvement in the inverse problem formulation [Eq. (13)] and its simple use when relying on the NNLS method. Another point of interest in employing this method resides in the formulation of the inverse problem. Equation (13) strongly suggests that once the scattering characteristics of the water content are known (along with the assumption that a single type of material dominates the scattering) and adequate frequencies are used to insonify the water column, it is possible to resolve both the concentration and the equivalent size distribution without any other observational input. This methodology could be of particular interest for continuous quantitative monitoring of suspended sediment, provided that continued efforts are made in refining the acoustic scattering characteristics of suspended sediments (e.g., in controlled environments), especially with respect to the flocculation of marine sediments.

b. *Inversion results*

Each profile of multifrequency acoustic measurements was inverted using the designed model and the NNLS method. The results are consistent in terms of total mass concentration estimates, fitting well to the in-situ observations. The optimum porosities used to invert the ABS signals are close to the ones observed at the water–sediment interface in 2009 during the same sampling periods (Khalil et al. 2013). They seem at least to highlight a seasonal contrast between the two experiments, with a mean porosity of 0.85 for the July experiment and 0.87 for the January experiment. It is worth mentioning that a small change in the optimum porosity can cause errors up to several factors in the mass concentration estimate, as the density contrast between the particles and γ is close to 1 (Chu et al. 2000). For illustration, several fixed mean input porosities ranging from 0.80 to 0.93 with increments of $\Delta\Phi = 0.03$ were tested with the present dataset to evaluate the dispersion of the inversion results. A linear fit was then calculated over the inversion results using the least squares method, guaranteeing minimum RMS variations. The results of these tests are displayed over the present dataset in Fig. 12, showing that the higher the porosity, the more sensitive the inversion. This highlights the difficulties encountered in the resolution of the present inverse problem at hand in the case of flocculated sediments.

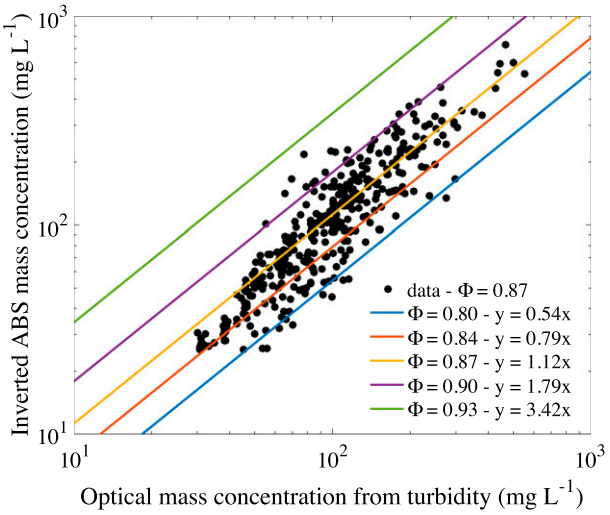

FIG. 12. Comparison between the optical turbidity converted into mass concentration (Fig. 3) and inverted mass concentration for several sets of porosity inputs for the January experiment. Each colored line represents the best fit of the inverted data for these porosity inputs [$\Phi = 0.93$ (green), 0.90 (purple), 0.87 (orange), 0.84 (red), and 0.80 (blue)], and the actual output of the inversion for the optimal Φ (0.87; black dots).

Given the atypical formulation of the backscattering model, when it comes to the size of the scatterers, a comparison between optical and acoustical observations is intricate. The solution of the acoustic inversion is distributed over a limited number of size classes of ESR of apparent particles, whereas the LISST observations deliver a straight representation of a volume distribution. A direct quantitative comparison would be subjective, as both methods provide different information. In terms of trend though, the radii evolution throughout the experiments presented by the LISST data (Fig. 6) and the inverted ABS data (Fig. 9) are in good agreement in July, exposing finer particles over the entire water column at the beginning of the experiment against a more stratified water column during the last three profiles at low tide slack water. For what concerns the attribution of the solution into the different ESR classes, some interesting features have been identified, especially near the low tide slack water in both experiments.

Two regimes can be identified (Figs. 6, 9, and 10). In the first regime (profiles 1–11 for the January experiment, and profiles 1–18 for the July experiment), only one dominant size mode of ESR is attributed as a solution of the inversion. The second regime (profiles 12–20 for the January experiment and 19–22 for the July experiment) sees another, larger dominant mode appear (ESR $> 150\,\mu$m for both experiments). These features are not thought to be the result of inversion artifacts, but rather the result of changes in scatterer characteristics.

Bigger aggregates are likely to be appearing, which is in accordance with the hydrodynamics conditions, especially during the January experiment, where a vertical salinity stratification is observed. These appearances are, however, likely to induce larger uncertainty in the final total mass concentration estimate, as some localized misfits between the estimated and observed mass concentrations were observed. Two probable causes of these misfit were identified:

1) The first one is thought to come from the global assumptions of the apparent scatterers in terms of shape and constitution: bigger material is unlikely to possess perfect spherical shapes, and thus a dependence on the scatterer orientation (given the high frequencies used here) relative to the transducers might be responsible for the misfits encountered in terms of total mass concentration during the January experiment, regardless of the aggregates density. With respect to the difference, a change in the material constitution is unlikely to be the main cause of these misfits: the results remain in good agreement with the mass concentrations observed (yet more dispersed: $R^2 = 0.81$ − RMS $= 24.6\,\mathrm{mg\,L^{-1}}$ for profiles 1–11, $R^2 = 0.74$ − RMS $= 61.6\,\mathrm{mg\,L^{-1}}$ for profiles 12–20) in spite of a ratio of density close to 1 (Chu et al. 2000). Besides, the experienced overestimation of the mass concentration coupled with the apparition of bigger material does not follow the evidence of a decreasing effective density with increasing size. This might therefore be the case during the last three profiles of the July experiment where a consequent underestimation of the total mass concentration is identified. No filtering has been applied to the acoustic data, and despite the appearance of this other dominant mode of scatterer, the results remain solid given the high natural variability encountered.
2) The second one concerns the limited size resolution and range of the NNLS method in terms of ESR, the size vector chosen for the acoustic inversion being logarithmically spaced. Under the assumption of fixed mean porosity averaged over the total size distribution, and thus considering apparent particles instead of physical particles, a small misattribution of the solution in higher size classes (accounting for the presence of bigger material) highly affects the final mass concentration estimate. Indeed, to a small number of large particles, corresponds a high mass concentration compared to the same number of small particles (Holliday and Pieper 1995). However, despite its qualitative substance in this context, the notion of ESR offers many advantages, a very interesting one being its capacity to be reduced to a unique estimate representing the entire suspension in terms of dominant scatterer, this without any information concerning its size distribution. Finally, in possession of such a piece of information about the suspension, and the associated backscattering model, it may become possible to retrieve the suspended sediment mass concentration using only one frequency without any assumptions about the particle size distribution.

c. *Flocculation dynamics*

The present experiments were carried out during ebb flow and lasted up to the beginning of low tide slack water. This time window was selected because it is likely to provide the opportunity to observe mass concentration variations sufficiently high enough (Bassoullet 1979) to successfully expose the current inverse problem. No data were collected afterward. During the July experiment, a clear size contrast has been identified, in accordance with an expected change in flocculation state due to favorable turbulence conditions (Manning et al. 2011). In the present study, and most specifically for what concerns the last four profiles of the July experiment, a higher porosity value appears to be most appropriate to describe the suspended matter, accounting for a significant drop in effective density. This highlights the fact that the relation featuring the steadiness of the mean porosity averaged over the total size distribution (Fig. 4) is likely to evolve given the tidal conditions. In particular, this change could be taken into account in this particular case by a distinction between flood/ebb periods and slack tide periods. This approach means discretizing the flocculation state, which reduces at first order to discriminating unimodal (microflocs) populations and multimodal (microflocs and macroflocs) populations, before tending toward a fractal approach as the core definition of the floc dynamics (Kranenburg 1994).

An example of such an approach is presented in Fig. 13 for the July experiment dataset, where the last four ABS profiles, corresponding to the slack tide period of the experiment, were inverted using a higher mean fixed porosity, 0.88, instead of 0.85. Increasing the porosity for these profiles yields estimates of the mass concentrations in better agreement with the observed in situ mass concentration.

Finally, these assumptions address two different complex problems, dealing with the expression of natural floc properties in both acoustics and hydrodynamics fields. Such assumptions are thus likely to lead to potentially significant uncertainties regarding mass concentration and size quantifications. Yet the exposed results remain in good agreement with in situ

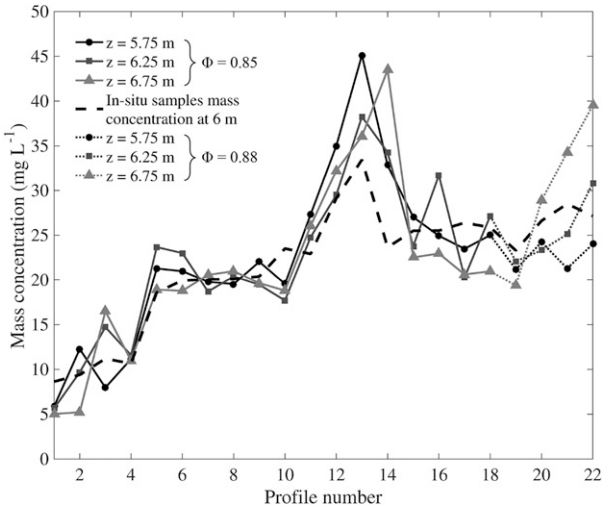

FIG. 13. Output of the inversion using the modified high-pass model for the July experiment at sampling depths with an applied constant $\Phi = 0.85$ (black lines) for profiles 1–18 (ebb) and $\Phi = 0.88$ (gray lines) for profiles 19–22 (slack tide). Profiles are for $z = 5.75$ m (circles), 6.25 m (squares), and 6.75 m (triangles).

observations given the high degree of natural variability encountered, the handling of which still represents a major challenge nowadays. In addition, the proposed approach appears promising with respect to continuous acoustic monitoring of the suspended aggregated sediment load.

To conclude, the present study underlines the need to improve measurement techniques and theoretical considerations regarding the description of natural floc properties, which remains challenging (Fettweis 2008; Verney et al. 2011; Thorne et al. 2014), so a finer description of in situ water masses of estuarine and coastal systems can be achieved.

d. Conclusions

In this paper, an absolute inversion of the in situ acoustic signal recorded at 0.5, 1, 2, and 4 MHz from aggregated particles in a macrotidal estuary is proposed by assuming they can be approximated by apparent particles of fixed low density. A backscattering model is proposed given an initial assumption of steady mean porosity averaged over the total size distribution. This assumption, inferred thanks to independent LISST data, enables the reduction from several degrees of freedom with poorly known parameters to an adjustable while coarsely bounded parameter, which helps constrain the shape of the backscattering model by describing the properties of apparent particles accounting for the suspension. The presented model was used to invert the multifrequency acoustic data recorded at a fixed location in the Aulne estuary (Fig. 1) in July 2014 and January 2015 using the nonnegative least squares algorithm. The inversion results are in good agreement with the in-situ mass concentration, covering concentration values from 15 to more than 500 mg L^{-1}. As long as a relative steadiness of the mean porosity averaged over the total size distribution is observed, this method is thought to be successful for material of a reasonable size ($a < 200\,\mu$m). The use of adapted frequencies is also highly recommended to avoid spanning too far into the geometric regime. Other experiments were successfully conducted in the same area in January 2014, May 2014, and March 2015. Nevertheless, future experiments should be conducted in different situations, and with aggregates of different constitutions, sizes, and effective densities, and complementary investigations should be carried out to highlight the use of the mean porosity of estuarine suspensions as a fluid apparent property. Finally, this study suggests that multifrequency ABS devices can operate as stand-alone systems to resolve both concentration and equivalent size distribution if the suspended material scattering properties are known, and it strongly encourages further development of theoretical and/or heuristic models to widen the potential applications of the quantitative use of acoustics in the sediment transport community.

Acknowledgments. This work was conducted in the framework of the ANR EPURE project (Grant 11 CEPL 005 02). This work was also supported by the Laboratoire d'Excellence LabexMER (ANR-10-LABX-19) and cofunded by a grant from the French government under the program Investissements d'Avenir. Romain Cancouët, Christophe Martin, Olivier Blanpain, Susane Moskalsky, Paul Juby, and Marcaurelio Franzetti were the keys to the success of the field measurements and laboratory work. The authors thank the Direction Générale de l'Armement (DGA), the Centre National de le Recherche Scientifique (CNRS), and l'Université de Bretagne Occidentale (UBO) for their funding of G. F.'s doctorate. The authors would also like to thank the Institut de la Recherche pour le Développement (IRD) for the use of their instruments and data, and for the help and support of their employees at land and at sea. Last but not least, we thank the Pôle Image team and the R/V *Albert Lucas* crew for their effective cooperation and support during the missions, with particular attention to Franck Quéré, Alban De Araujo, and Daniel Morigeon.

REFERENCES

Agrawal, Y. C., and H. C. Pottsmith, 2000: Instruments for particle size and settling velocity observations in sediment transport. *Mar. Geol.*, **168**, 89–114, doi:10.1016/S0025-3227(00)00044-X.

Allen, G. P., J. C. Salomon, P. Bassoullet, Y. Du Penhoat, and C. De Grandpre, 1980: Effects of tides on mixing and suspended sediment transport in macrotidal estuaries. *Sediment. Geol.*, **26**, 69–90, doi:10.1016/0037-0738(80)90006-8.

Amoudry, L. O., and A. J. Souza, 2011: Deterministic coastal morphological and sediment transport modeling: A review and discussion. *Rev. Geophys.*, **49**, RG2002, doi:10.1029/2010RG000341.

Andrews, S. W., D. M. Nover, and S. G. Schladow, 2010: Using laser diffraction data to obtain accurate particle size distributions: The role of particle composition. *Limnol. Oceanogr. Methods*, **8**, 507–526, doi:10.4319/lom.2010.8.507.

——, ——, J. E. Reuter, and S. G. Schladow, 2011: Limitations of laser diffraction for measuring fine particles in oligotrophic systems: Pitfalls and potential solutions. *Water Resour. Res.*, **47**, 1–12, doi:10.1029/2010WR009837.

Bassoullet, P., 1979: Étude de la dynamique des sédiments en suspension dans l'estuaire de l'Aulne (Rade de Brest) [Study of the suspended sediment dynamics in the Aulne estuary (Brest Bay)]. Ph.D. thesis, Université de Bretagne Occidentale, 136 pp.

Betteridge, K. F. E., P. D. Thorne, and R. D. Cooke, 2008: Calibrating multi-frequency acoustic backscatter systems for studying near-bed suspended sediment transport processes. *Cont. Shelf Res.*, **28**, 227–235, doi:10.1016/j.csr.2007.07.007.

Bilotta, G. S., and R. E. Brazier, 2008: Understanding the influence of suspended solids on water quality and aquatic biota. *Water Res.*, **42**, 2849–2861, doi:10.1016/j.watres.2008.03.018.

Buckingham, M. J., 2005: Compressional and shear wave properties of marine sediments: Comparisons between theory and data. *J. Acoust. Soc. Amer.*, **117**, 137–152, doi:10.1121/1.1810231.

Castagna, J. P., M. L. Batzle, and R. L. Eastwood, 1985: Relationship between compressional-wave and shear wave velocities in clastic silicate rocks. *Geophysics*, **50**, 571–581, doi:10.1190/1.1441933.

Chen, C. T., and F. J. Millero, 1977: Speed of sound in seawater at high pressures. *J. Acoust. Soc. Amer.*, **62**, 1129–1135, doi:10.1121/1.381646.

Chu, D., P. H. Wiebe, and N. J. Copley, 2000: Inference of material properties of zooplankton from acoustic and resistivity measurements. *ICES J. Mar. Sci.*, **57**, 1128–1142, doi:10.1006/jmsc.2000.0800.

Cox, M. J., T. B. Letessier, and A. S. Brierley, 2013: Zooplankton and micronekton biovolume at the Mid-Atlantic Ridge and Charlie–Gibbs Fracture Zone estimated by multi-frequency acoustic survey. *Deep-Sea Res. II*, **98**, 269–278, doi:10.1016/j.dsr2.2013.07.020.

Crawford, A. M., and A. E. Hay, 1993: Determining suspended sand size and concentration from multifrequency acoustic backscatter. *J. Acoust. Soc. Amer.*, **94**, 3312–3324, doi:10.1121/1.407237.

Davies, A. G., and P. D. Thorne, 2008: Advances in the study of moving sediments and evolving seabeds. *Surv. Geophys.*, **29**, 1–36, doi:10.1007/s10712-008-9039-x.

Eisma, D., and A. Li, 1993: Changes in suspended-matter floc size during the tidal cycle in the Dollard estuary. *Neth. J. Sea Res.*, **31**, 107–117, doi:10.1016/0077-7579(93)90001-9.

Fettweis, M., 2008: Uncertainty of excess density and settling velocity of mud flocs derived from in situ measurements. *Estuarine Coastal Shelf Sci.*, **78**, 426–436, doi:10.1016/j.ecss.2008.01.007.

Francois, R. E., and G. R. Garrison, 1982: Sound absorption based on ocean measurements. Part II: Boric acid contribution and equation for total absorption. *J. Acoust. Soc. Amer.*, **72**, 1879–1890, doi:10.1121/1.388673.

Gartner, J. W., R. T. Cheng, P. F. Wang, and K. Richter, 2001: Laboratory and field evaluations of the LISST-100 instrument for suspended particle size determinations. *Mar. Geol.*, **175**, 199–219, doi:10.1016/S0025-3227(01)00137-2.

Gray, J. R., and J. W. Gartner, 2009: Technological advances in suspended-sediment surrogate monitoring. *Water Resour. Res.*, **45**, W00D29, doi:10.1029/2008WR007063.

Greenlaw, C. F., 1979: Acoustical estimation of zooplankton populations. *Limnol. Oceanogr.*, **24**, 226–242, doi:10.4319/lo.1979.24.2.0226.

——, and R. K. Johnson, 1983: Multiple-frequency acoustical estimation. *Biol. Oceanogr.*, **2**, 227–252, doi:10.1080/01965581.1983.10749460.

Hamilton, E. L., 1963: Sediment sound velocity measurements made in situ from bathyscaph *Trieste*. *J. Geophys. Res.*, **68**, 5991–5998, doi:10.1029/JZ068i021p05991.

Han, D. H., A. Nur, and A. D. Morgan, 1986: Effect of porosity and clay content on wave velocities in sandstones. *Geophysics*, **51**, 2093–2107, doi:10.1190/1.1442062.

Hay, A. E., 1991: Sound scattering from a particle-laden, turbulent jet. *J. Acoust. Soc. Amer.*, **90**, 2055–2074, doi:10.1121/1.401633.

Holliday, D. V., and R. E. Pieper, 1995: Bioacoustical oceanography at high frequencies. *ICES J. Mar. Sci.*, **52**, 279–296, doi:10.1016/1054-3139(95)80044-1.

——, ——, and G. S. Kleppel, 1989: Determination of zooplankton size and distribution with multifrequency acoustic technology. *ICES J. Mar. Sci.*, **46**, 52–61, doi:10.1093/icesjms/46.1.52.

Hwang, B. K., M. Furusawa, and M. Ogata, 2007: Validation of multi-frequency inversion method by using dummy scatterers of zooplankton. *Fish. Sci.*, **73**, 250–262, doi:10.1111/j.1444-2906.2007.01331.x.

Johnson, R. K., 1977: Acoustic estimation of scattering-layer composition. *J. Acoust. Soc. Amer.*, **61**, 1636–1639, doi:10.1121/1.381440.

Khalil, K., and Coauthors, 2013: Spatial and temporal variability of sediment organic matter recycling in two temperate eutrophicated estuaries. *Aquat. Geochem.*, **19**, 517–542, doi:10.1007/s10498-013-9213-8.

Kranenburg, C., 1994: The fractal structure of cohesive sediment aggregates. *Estuarine Coastal Shelf Sci.*, **39**, 451–460, doi:10.1016/S0272-7714(06)80002-8.

Lawson, C. L., and R. J. Hanson, 1974: *Solving Least Squares Problems*. Prentice-Hall, 337 pp.

Lawson, G. L., P. H. Wiebe, T. K. Stanton, and C. J. Ashjian, 2008: Euphausiid distribution along the Western Antarctic Peninsula—Part A: Development of robust multi-frequency acoustic techniques to identify euphausiid aggregations and quantify euphausiid size, abundance, and biomass. *Deep-Sea Res. II*, **55**, 412–431, doi:10.1016/j.dsr2.2007.11.010.

Lebourges-Dhaussy, A., 1996: Caractérisation des populations planctoniques par acoustique multifréquence (Characterization of planktonic populations using multifrequency acoustics). *Oceanis*, **22**, 71–92.

——, J. Hugget, S. Ockhuis, G. Roudaut, E. Josse, and H. Verheye, 2014: Zooplankton size and distribution within mesoscale structures in the Mozambique Channel: A comparative approach using the TAPS acoustic profiler, a multiple net sampler and ZooScan image analysis. *Deep-Sea Res. II*, **100**, 136–152, doi:10.1016/j.dsr2.2013.10.022.

MacDonald, I. T., C. E. Vincent, P. D. Thorne, and B. D. Moate, 2013: Acoustic scattering from a suspension of flocculated

sediments. *J. Geophys. Res. Oceans*, **118**, 2581–2594, doi:10.1002/jgrc.20197.

Maclennan, D. N., P. G. Fernandes, and J. Dalen, 2002: A consistent approach to definitions and symbols in fisheries acoustics. *ICES J. Mar. Sci.*, **59**, 365–369, doi:10.1006/jmsc.2001.1158.

Manning, A. J., J. V. Baugh, R. L. Soulsby, J. R. Spearman, and R. J. S. Whitehouse, 2011: Cohesive sediment flocculation and the application to settling flux modelling. *Sediment Transport*, S. S. Ginsberg, Ed., InTech, 91–116, doi:10.5772/16055.

Medwin, H., and C. S. Clay, 1997: *Fundamentals of Acoustical Oceanography*. Academic Press, 712 pp.

Mikkelsen, O. A., T. G. Milligan, P. S. Hill, R. J. Chant, C. F. Jago, S. E. Jones, V. Krivtsov, and G. Mitchelson-Jacob, 2008: The influence of schlieren on in situ optical measurements used for particle characterization. *Limnol. Oceanogr. Methods*, **6**, 133–143, doi:10.4319/lom.2008.6.133.

Moate, B. D., and P. D. Thorne, 2009: Measurements and inversion of acoustic scattering from suspensions having broad size distributions. *J. Acoust. Soc. Amer.*, **126**, 2905–2917, doi:10.1121/1.3242374.

Sequoia Inc., 2008: Processing LISST-100 and LISST-100X data in MATLAB. [Available online at http://www.sequoiasci.com/article/processing-lisst-100-and-lisst-100x-data-in-matlab/.]

Sheng, J., and A. E. Hay, 1988: An examination of the spherical scatterer approximation in aqueous suspensions of sand. *J. Acoust. Soc. Amer.*, **83**, 598–610, doi:10.1121/1.396153.

Smerdon, A. M., J. M. Rees, and C. E. Vincent, 1998: An acoustic backscatter instrument to measure near-bed sediment processes. Aquatec Electronics Ltd., 19 pp.

Stanton, T. K., 1989: Simple approximate formulas for backscattering of sound by spherical and elongated objects. *J. Acoust. Soc. Amer.*, **86**, 1499–1510, doi:10.1121/1.398711.

——, P. H. Wiebe, and D. Chu, 1998: Differences between sound scattering by weakly scattering spheres and finite-length cylinders with applications to sound scattering by zooplankton. *J. Acoust. Soc. Amer.*, **103**, 254–264, doi:10.1121/1.421135.

Styles, R., 2006: Laboratory evaluation of the LISST in a stratified fluid. *Mar. Geol.*, **227**, 151–162, doi:10.1016/j.margeo.2005.11.011.

Thorne, P. D., and P. J. Hardcastle, 1997: Acoustic measurements of suspended sediments in turbulent currents and comparison with in-situ samples. *J. Acoust. Soc. Amer.*, **101**, 2603–2614, doi:10.1121/1.418501.

——, and D. M. Hanes, 2002: A review of acoustic measurement of small-scale sediment processes. *Cont. Shelf Res.*, **22**, 603–632, doi:10.1016/S0278-4343(01)00101-7.

——, P. J. Hardcastle, and R. L. Soulsby, 1993: Analysis of acoustic measurements of suspended sediments. *J. Geophys. Res.*, **98**, 899–910, doi:10.1029/92JC01855.

——, D. Hurther, and B. D. Moate, 2011: Acoustic inversions for measuring boundary layer suspended sediment processes. *J. Acoust. Soc. Amer.*, **130**, 1188–1200, doi:10.1121/1.3618728.

——, I. T. MacDonald, and C. E. Vincent, 2014: Modelling acoustic scattering by suspended flocculating sediments. *Cont. Shelf Res.*, **88**, 81–91, doi:10.1016/j.csr.2014.07.003.

Traykovski, P., R. J. Latter, and J. D. Irish, 1999: A laboratory evaluation of the laser in situ scattering and transmissometery instrument using natural sediments. *Mar. Geol.*, **159**, 355–367, doi:10.1016/S0025-3227(98)00196-0.

Uncles, R. J., J. A. Stephens, and D. J. Law, 2006: Turbidity maximum in the macrotidal, highly turbid Humber Estuary, UK: Flocs, fluid mud, stationary suspensions and tidal bores. *Estuarine Coastal Shelf Sci.*, **67**, 30–52, doi:10.1016/j.ecss.2005.10.013.

Verney, R., R. Lafite, J.-C. Brun-Cottan, and P. Le Hir, 2011: Behaviour of a floc population during a tidal cycle: Laboratory experiments and numerical modelling. *Cont. Shelf Res.*, **31**, S64–S83, doi:10.1016/j.csr.2010.02.005.

Wood, A. B., 1964: *A Textbook of Sound: Being an Account of the Physics of Vibrations with Special Reference to Recent Theoretical and Technical Developments*. 3rd ed. George Bell & Sons Ltd., 610 pp.